Supplementary Information (SI) for Materials Chemistry Frontiers.
This journal is © the Partner Organisations 2026

Diazadioxa[8]circulene – A platform for stable antiaromatic radicals with strong NIR absorption

Cecilia Bruschi,[a, b,†] Ihor Sahalianov,[a, b,†] Yuri Tanuma,[a] Levani Skhirtladze,[a] Rashid Valiev,[c] Xinyi Cai,[d] Feng Gao,[d] Mikhail Vagin,[a, b] Yann Lie,[e] Michael Pittelkow, [e] Renee Kroon,[a, b,*] Glib Baryshnikov[a, b,*]

[a]Department of Science and Technology, Laboratory of Organic Electronics, Linköping University, SE-60174, Norrköping, Sweden. E-mail: glib.baryshnikov@liu.se

[b]Wallenberg Initiative Materials Science for Sustainability, Department of Science and Technology, Linköping University SE-60174, Norrköping, Sweden

[c]Department of Chemistry, Faculty of Science, University of Helsinki, P. O. Box 55 (A. I. Virtanens plats 1), Finland

[d]Department of Physics, Chemistry and Biology (IFM), Linköping University, SE-581 83, Linköping, Sweden

[e]Department of Chemistry, University of Copenhagen, Universitetsparken 5, Copenhagen Ø, DK-2100, Denmark

[†] Authors contributed equally to the work

Table of Contents

Materials and Methods....2
Synthesis....3
FTIR analysis....4
EPR analysis....4
Vis-NIR spectroscopy....6
Stability tests....7
Single-crystal electron diffraction....9
Spectroelectrochemistry....12
Faradaic efficiency....13
Theoretical calculations....16

Materials and Methods

General

Tris(4-bromophenyl)ammoniumyl hexachloroantimonate was purchased by Sigma Aldrich and used without further purification.

The starting diazadioxa[8]circulene **C1** compound was synthesized according to previously published procedure.[1]

Absorption spectra measurements in solution and in solid state

For the Vis-NIR absorption spectra in solution, spectroscopy gradient dichloromethane solvent was used. For the measurement in solid state, 1 mg of the product and 99 mg of PMMA were dissolved in 4 mL of dichloromethane. Then 1 mL of the resulting dispersion was drop-casted on a glass slide and the solvent was let to evaporate slowly overnight. The instrument used for measuring the absorption spectra in both the dissolved and solid state was a fiber optic spectrometer, equipped with AvaLight-DH-S-BAL (Halogen and Deuterium lamps, 215-2500 nm range) and AvaLight-HAL-S-Mini (Halogen lamp, 360-2500 nm range) as light sources and with AvaSpec-NIR (1000-2500 nm) and AvaSpec-2048L (200-1100 nm) as detectors.

Electrochemistry

For all the electrochemical measurements a Biologic SP299 potentiostat was used. For the cyclic voltammetry, a glassy carbon disk was used as working electrode and two Pt wires were used as counter and reference electrodes. The ferrocene Fc/Fc^+ couple was used as internal standard. Tetrabutylammonium hexafluorophosphate ($TBAPF_6$) 0.1 M was used as supporting electrolyte.

Spectroelectrochemistry

The Vis-NIR spectroelectrochemistry was performed using 10 mm quartz cuvette and dissolving the circulene **C1** in 0.1 M $TBAPF_6$ dichloromethane solutions. A Pt honeycomb electrode (Pine Research Instrumentation Inc., USA) was adopted for the working and counter electrodes and a Pt wire was used as reference electrode. Chronoamperometry measurements were performed using a Biologic SP299 potentiostat and the spectra were recorded using a fiber optic spectrometer equipped with AvaLight-HAL-S-Mini as light source and AvaSpec-NIR, AvaSpec-2048L as detectors. All the potentials are reported versus ferrocene couple Fc/Fc+ and all the spectra are reported in terms of differential absorption ΔA, where A_0 represents the spectra measured without applying any potential.

EPR experimental analysis

EPR spectra were measured in solution and at room temperature using a SPINSCAN X instrument. Dichloromethane was used as solvent for the circulene **C1** and the radical cation **R1**, while acetonitrile was used for Magic Blue.

Simulation of EPR spectra

All simulation of EPR spectra were performed by using the garlic function in EasySpin package (version 6.0.6).[45]

DFT calculations for EPR parameters

EPR parameters of the pre-optimised structure were calculated at B3LYP[31-33]/EPR-II by using ORCA package (version 6.0).[46,47,48]

FTIR

FTIR spectra were recorded analyzing powders with a PerkinElmer Spectron 3.

Synthesis

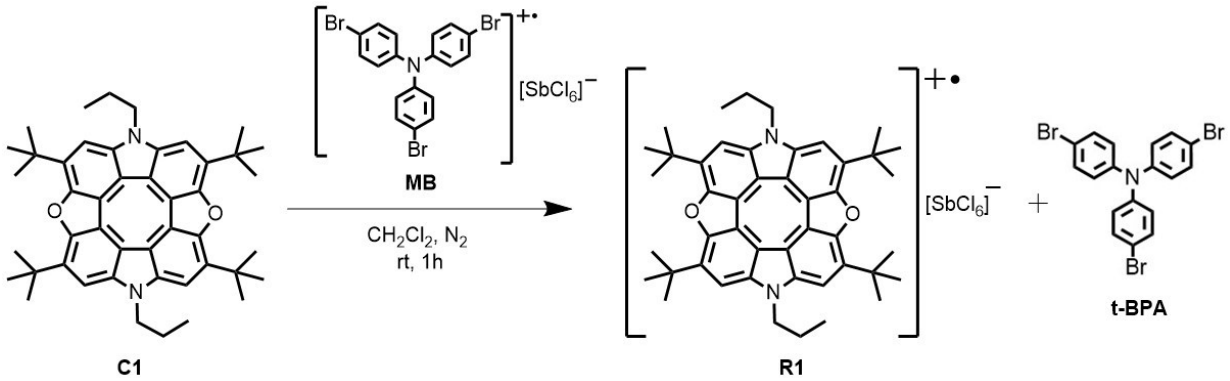

Figure S1. Reaction scheme of the synthesis of the circulene radical cation **R1** by oxidation of the diazadioxa[8]circulene **C1** with Magic Blue, including the chemical structure of the coproduct tris(4-bromophenyl)amine (**t-BPA**).

The starting diazadioxa[8]circulene **C1** (30 mg, 0.045 mmol, 1 equiv.) was reacted with tris(4-bromophenyl)ammoniumyl hexachloroantimonate (44 mg, 0.054 mmol, 1.2 equiv.) in 10 mL of dichloromethane, under N_2 atmosphere. After stirring for one hour at room temperature, the crude was purified adding an excess of n-hexane to a concentrated solution of dichloromethane. The product was precipitated, and the supernatant solution was removed. The remaining solvent was removed by vacuum. The procedure was repeated at least twice, and the purity was monitored by spectroscopy measurements. The product was isolated as a red powder. 38 mg (Yield: 84 %)

FTIR analysis

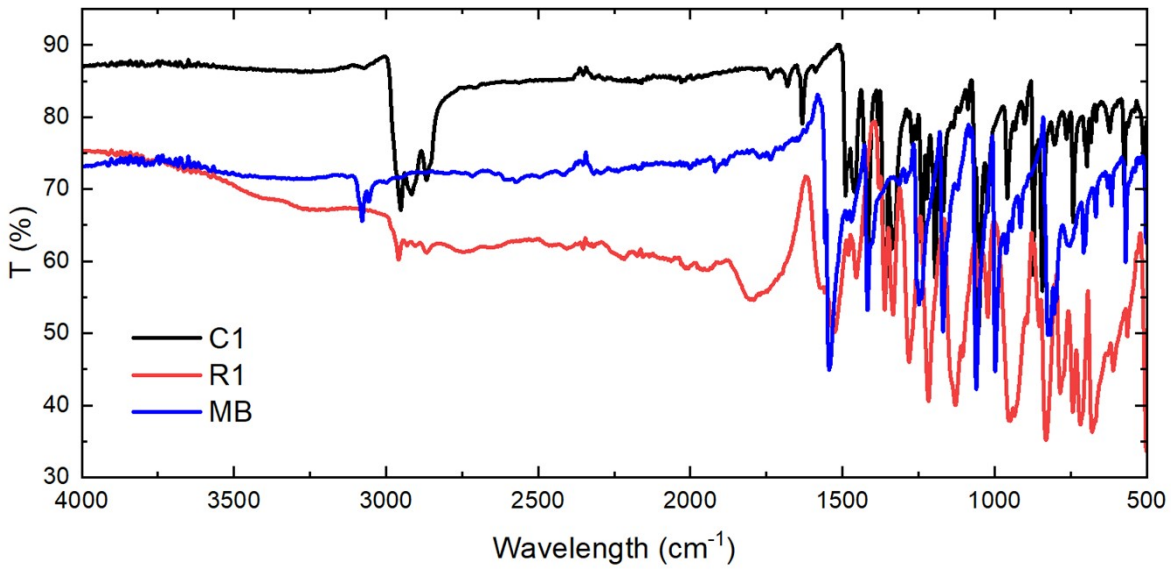

Figure S2. Comparison of the FTIR spectra of the starting circulene **C1** (black line), of the Magic Blue (blue line) and of the radical cation product **R1** (red line). The product shows new peaks in the 2000-500 nm range, which are absent in both the starting materials.

EPR analysis

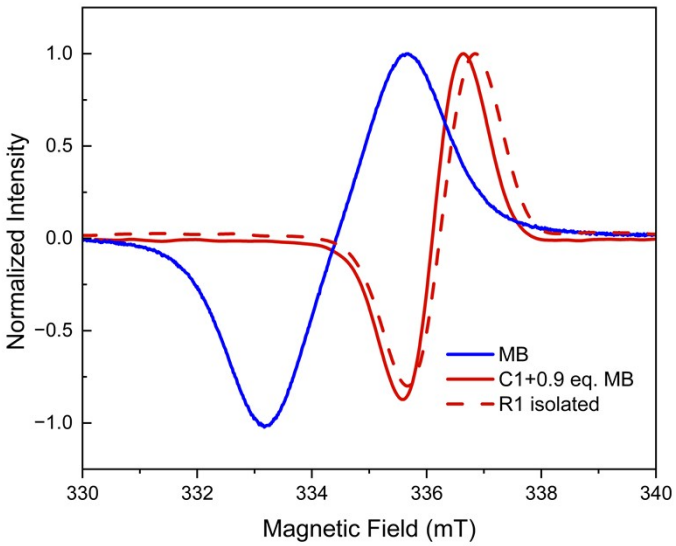

Figure S3. EPR spectra of a dichloromethane le solution of Magic Blue (blue line), of the product **R1** isolated after large-scale reaction (dashed red line), of the solution product obtained by directly mixing the starting material with 0.9 equivalent of Magic Blue (solid red line

Table S1. EPR parameters obtained from the curve fitting of the experimental spectrum. “FWHM” stands for full width at half maximum. ”ci95” is 95% confidence interval.

EPR parameters	*g*-factor	A^{N}_{iso} [MHz]	A^{H}_{iso} [MHz]	FWHM (Gaussian)	FWHM (Lorentzian)
Best fitting value	2.0079	6.13	8.51	0.41	0.17
Lower ci95	2.0079	6.1248	8.5017	0.3405	0.1242
Upper ci95	2.0079	6.1420	8.5185	0.4838	0.2239

Table S2. Summary of DFT-calculated hyperfine coupling constants. For hydrogen, the four atoms attached to the [8]circulene ring are listed. Atomic labels correspond to the ones in Figure 2a.

Atom	**A_x [MHz]**	**A_y [MHz]**	**A_z [MHz]**	**A_{iso} [MHz]**
1N	23.28	0.97	1.15	8.47
2N	23.17	0.97	1.14	8.43
3H	-10.48	-3.90	-14.50	-9.63
4H	-10.46	-3.89	-14.47	-9.61
5H	-10.36	-3.87	-14.31	-9.51
6H	-10.38	-3.88	-14.33	-9.53

Vis-NIR spectroscopy

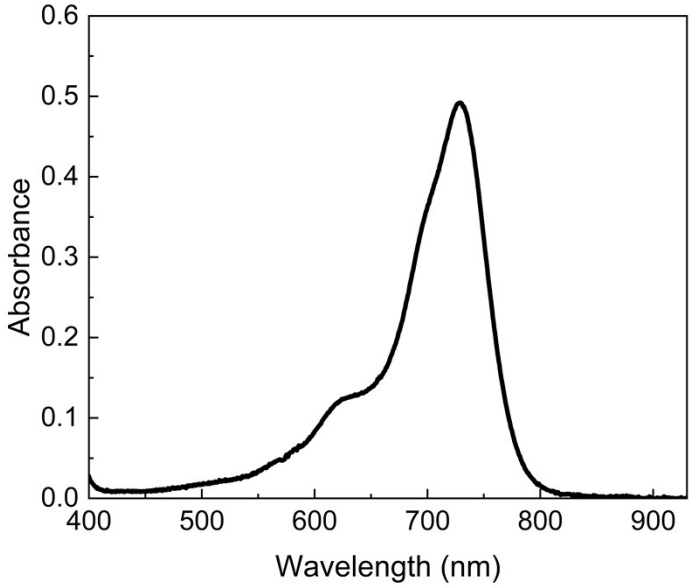

Figure S4. Absorption spectrum of a solution of tris(4-bromophenyl)ammoniumyl hexachloroantimonate (Magic blue) in dichloromethane ([c] = $7*10^{-6}$ M).

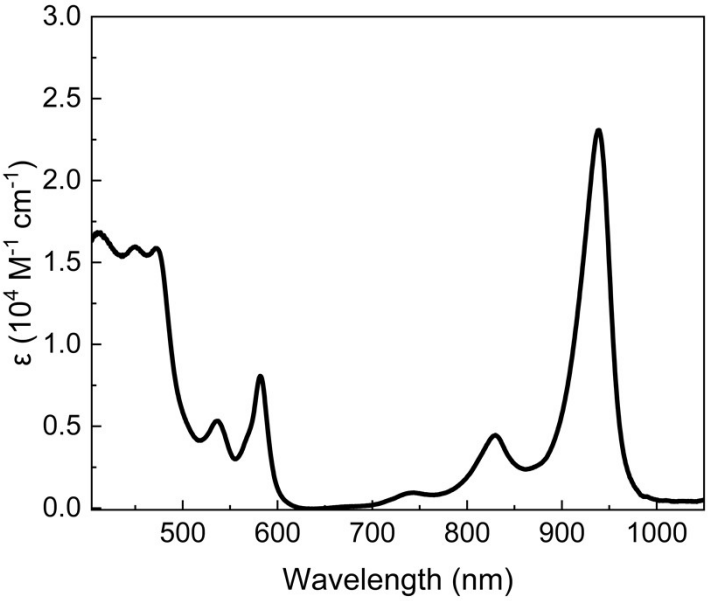

Figure S5. Absorption spectrum of the isolated radical cation **R1** in dichloromethane solution.

To detect the absorption spectrum of the radical circulene in the solid state, a film of the radical cation dispersed in a polymethyl methacrylate (PMMA) matrix at 1.0% w/w was prepared. The absorption spectrum of the solid state (Figure S6) is slightly blue-shifted with respect to that solution, showing a peak in the NIR at 924 nm (ΔE= 0.02 eV).

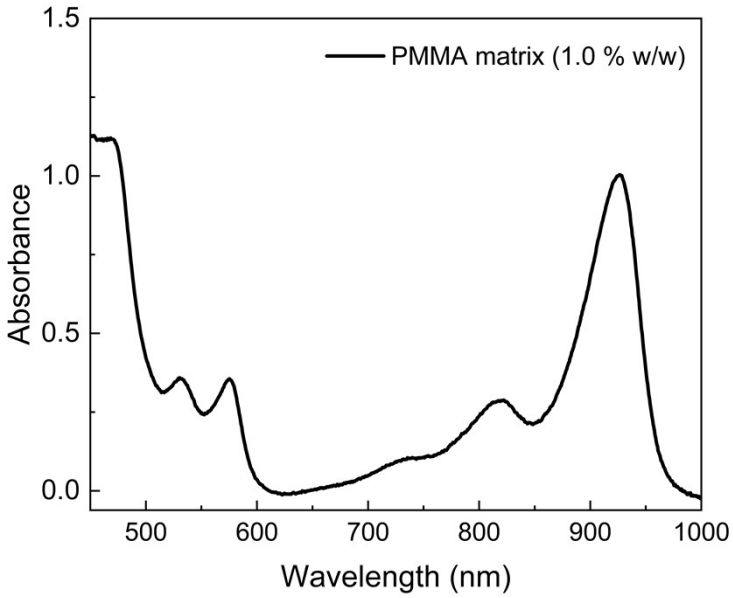

Figure S6. Normalized absorption spectrum of the radical cation **R1** in PMMA matrix (1.0 % w/w).

Stability tests

The radical cation is moderately stable in solution. However, overtime a gradual reformation of the neutral circulene **C1** is observed, as indicated by the appearance and intensification of its peaks at 402 and 420 nm (Figure S7, red box). Really important is the purity of the solvent chosen for dissolving the radical cation. Indeed, a higher percentage of the reformed starting material is observed using a 99.5% dichloromethane compared to the spectroscopic gradient one, probably due to a higher presence of stabilizers like amylene that can be potentially reactive towards the radical (Figure S8).

The radical cation is notably stable also in the solid state. Indeed, only a small increase in the circulene peaks are observed after days (Figure S8). It is important to note that in this case the peak of the circulene is already present in the first spectra measured for the film of the radical cation in PMMA matrix (black line, Figure S8). This result may be attributable to the method of preparation of the film: 1 mL solution was drop-casted on a glass slide and the solvent slowly evaporated overnight, which allowed one part of the product to be converted back to the starting material.

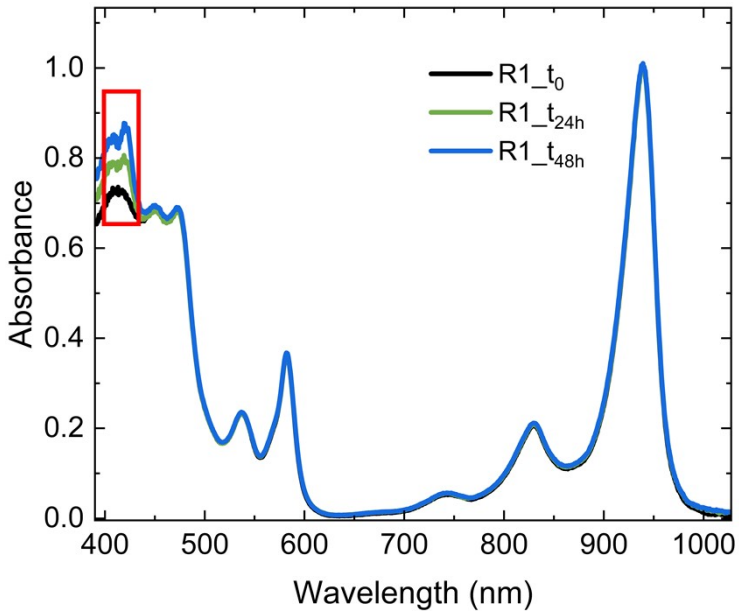

Figure S7. Normalized absorption spectra of the radical cation **R1** measured overtime. The appearance and intensification of the peaks at 402 and 420 nm, attributed to the starting material **C1**, are highlighted by the red box. The spectra are normalised at 939 nm due to dichloromethane evaporation.

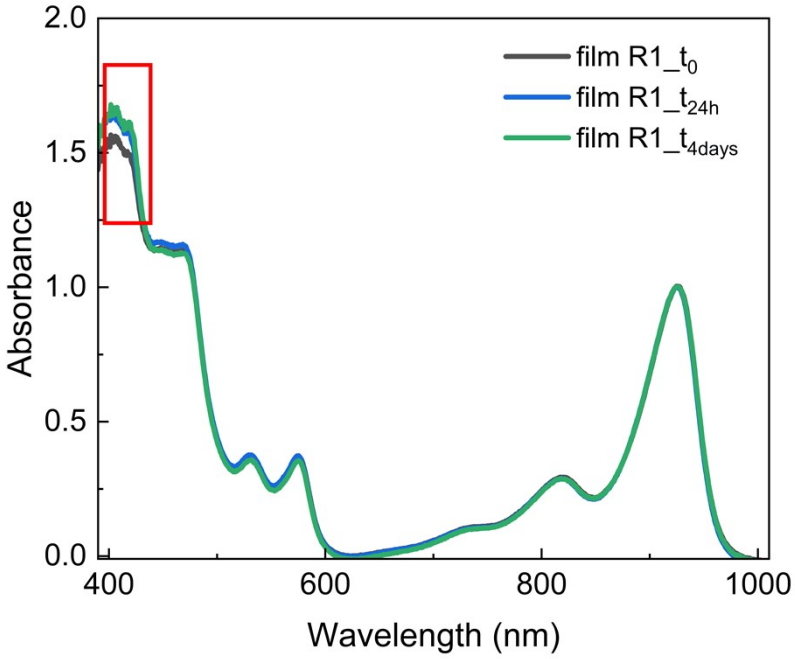

Figure S8. Normalized absorption spectra measured overtime for a film of the radical cation **R1** in PMMA matrix.

Single-crystal electron diffraction

Crystals of **R1** could only be grown to a size of few microns, and the structure was determined with 3D electron diffraction (3D ED). To this end a 200-mesh copper TEM grid coated with a continuous film of amorphous carbon (from EMS) was shaken in a vial containing the dried powder. 3D ED experiments were performed at 173 K in high vacuum on a Rigaku XtaLAB Synergy-ED, equipped with a LaB_6 source operating at 200 kV (λ = 0.0251 Å) and a Rigaku HyPix-ED detector. The sample grid was with a Gatan Elsa cryoholder. Series of diffraction patterns were collected on 5 crystals during continuous rotation of the specimen. Selected area apertures with an apparent diameter of 1 or 2 µm were used to delimit the diffracting region of the crystals. The program CrysAlis Pro (1.171.44.122a)[49] was used to control the data collection and multiple illumination conditions, detector distances and data collection parameters were tested to improve the data quality.

The crystal structure was solved ab initio with SHELXT[50] using Olex2.[51] The least-squares refinement in kinematic approximation was carried out with SHELXL,[52] using the scattering factors for electrons.[53] The positions of all atoms of the circulene core were refined freely. The *t*Bu and Pr side groups are slightly disordered and soft restraints were applied to maintain a consistent geometry and to mitigate for the low data/parameter ratio. An extinction parameter was refined to mitigate the effects of multiple diffraction. Anisotropic displacement parameters were refined for non-hydrogen atoms, while H-atoms were placed in geometrically idealized position and refined with a riding model, using tabulated distances from neutron diffraction[54] and isotropic thermal parameters derived from the parent atom. Figures were made using ORTEP3[55] and Mercury.[56] Cif files were finalized using CIVET and FinalCif. The structure was deposited on the CCDC database identifier: 2494920.

Table S6. Crystal data and structure refinement for R1

Compound	Diazaoxa[8]circulene radical cation (**R1)**
CCDC number	2494920
Empirical formula	$C_{46}H_{54}N_2O_2SbCl_6$
Formula weight	1001.43
Temperature [K]	173
Crystal system	triclinic
Space group (number)	$P\bar{1}$ (2)
a [Å]	8.2398(6)
b [Å]	9.9107(10)
c [Å]	15.8890(7)
α [°]	78.883(6)
β [°]	76.898(5)
γ [°]	65.511(8)
Volume [Å^3]	1142.89(17)
Z	1
ρ_{calc} [gcm^{-3}]	1.455
μ [mm^{-1}]	0.000
F(000)	192
Crystal size [mm^3]	0.01×0.01×?
Crystal colour	clear brownish red
Crystal shape	plate
Radiation	electron (λ=0.0251 Å)
2θ range [°]	0.09 to 1.81 (0.80 Å)
Index ranges	−10 ≤ h ≤ 10 −12 ≤ k ≤ 12 −19 ≤ l ≤ 19
Reflections collected	25568
Independent reflections	4004 R_{int} = 0.1403 R_{sigma} = 0.0801
Completeness to θ = 0.863°	85.0 %
Data / Restraints / Parameters	4004 / 108 / 267
Absorption correction	multi-scan
Goodness-of-fit on F^2	1.128
Final *R* indexes [I≥2σ(I)]	R_1 = 0.1653 wR_2 = 0.4231
Final *R* indexes [all data]	R_1 = 0.1872 wR_2 = 0.4370
Largest peak/hole [eÅ^{-3}]	0.34/−0.30
Extinction coefficient	1700(20)

a)

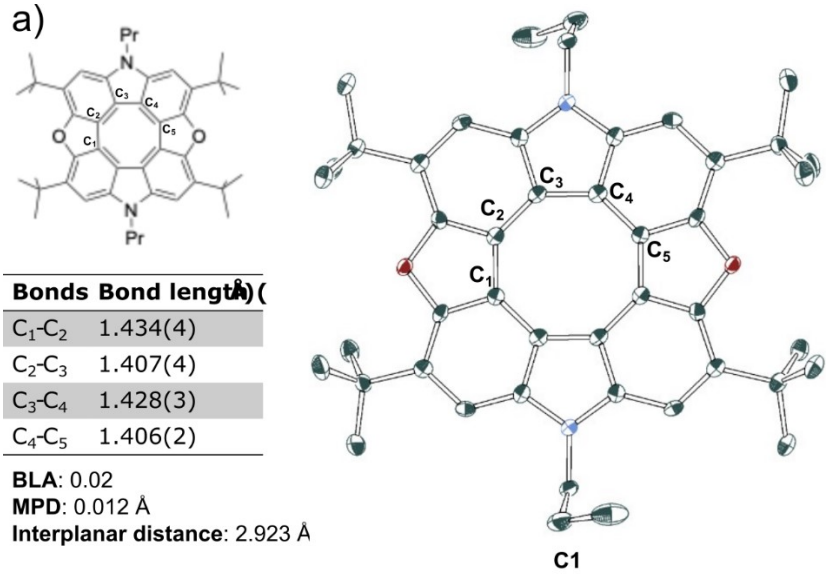

Bonds	Bond length(Å)
C_1-C_2	1.434(4)
C_2-C_3	1.407(4)
C_3-C_4	1.428(3)
C_4-C_5	1.406(2)

BLA: 0.02
MPD: 0.012 Å
Interplanar distance: 2.923 Å

C1

b)

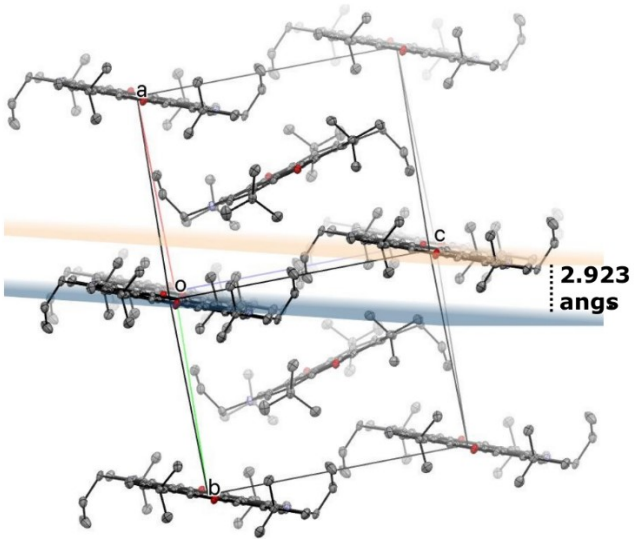

Figure S9. a) SC-XRD structure of C1 represented as ORTEP diagrams (CCDC: 945393) . the 50% thermal ellipsoids. Non-hydrogen atoms are represented as 50% probability thermal ellipsoids, and selected bond lengths are given in Å (uncertainty in brackets). Atoms are colored grey (carbon), red (oxygen), and blue (nitrogen). Hydrogens are omitted for clarity. b) Packing diagram of C1, interplanar distance between the residues is shown.

Spectroelectrochemistry

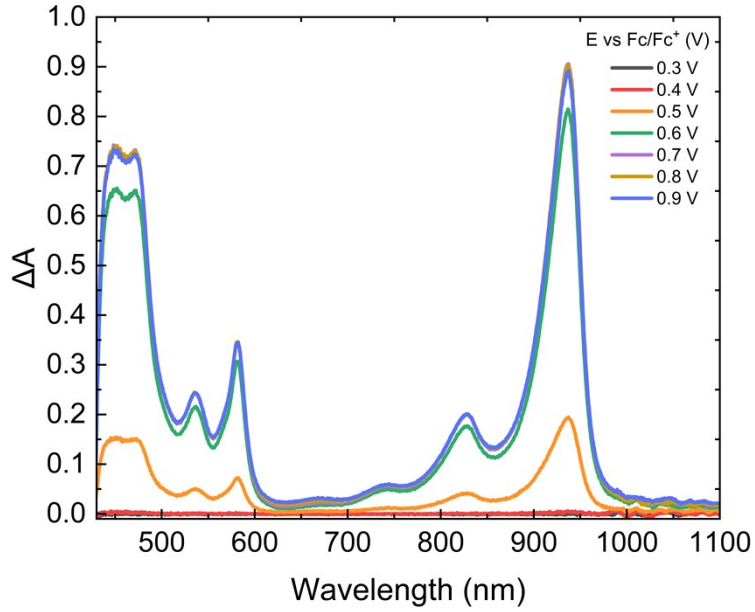

Figure S10. Differential absorption spectra of circulene **C1** measured using a honeycomb electrode after the application of an increasing potential from 0.3 V to 0.9 V (vs Fc/Fc^+) for 90 s. Prior to and following each potential, a potential of -0.1 V was applied for 30 s. The spectra reported were recorded after a 60 s interval.

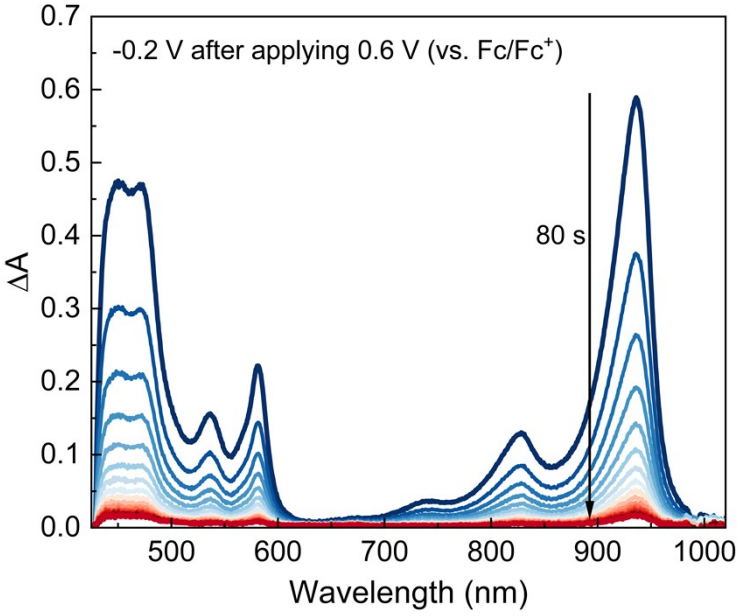

Figure S11. Evolution of the differential absorption spectrum of circulene **C1** applying a potential of -0.2 V for 80 s, subsequently the application of a potential of 0.6 V for 90 s.

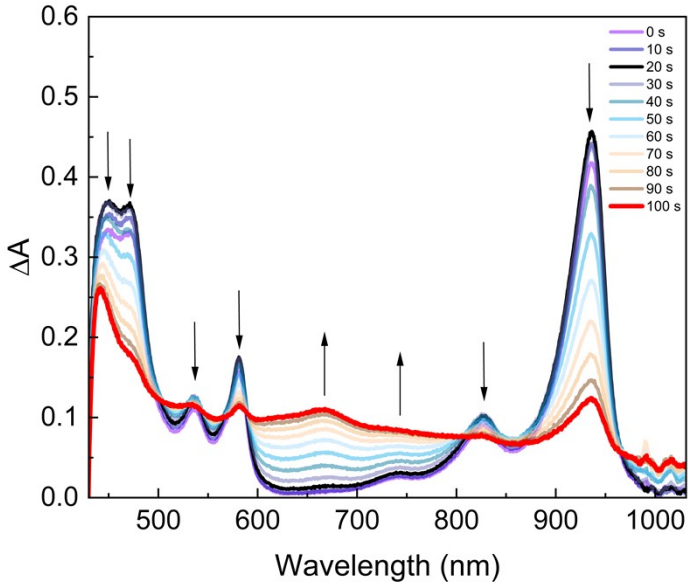

Figure S12. Differential absorption spectra of circulene **C1** measured applying potential of 1.2 V (vs. Fc/Fc^{+}) for 100 s, after applying 0.7 V for 60 s (0 s spectra, purple line); spectra were recorded at ten-seconds intervals. The final spectrum obtained is attributed to a mixture of the radical cation and the dication.

Faradaic efficiency

For the estimation of the faradaic efficiency, a previously published procedure was followed.[30] The faradaic efficiency represents the ratio between the number of moles of the studied compound that are converted and recorded by optical measurements (n_{optics}) and the number of moles of the same compound that are converted due to electrolysis ($n_{electrolysis}$):

$$\text{FE (\%)} = \frac{n_{optics}}{n_{electrolysis}}$$

The number of moles converted is calculated at the time when the starting material is almost completely consumed in the tabular cavities. At this point in the experiment the differential absorption at a specific wavelength changes from exhibiting an almost linear increase to a plateau, due to the change in the diffusion regime.

The n_{optics} is obtained by the product between the consumed/produced concentration (Δc_t) of the starting material/product at the saturation time t and the volume (V) of the electrode cavity: $n_{optics} = \Delta c_t * V$. Δc_t is calculated from the ΔA_t at 937 nm, close to the maximum absorption peak of the radical cation **R1** ($\Delta c_t = \Delta A_t / \varepsilon b$; b corresponds to the length of the tubular cavities of 0.17 cm). Considering that the honeycomb consists of 19 tubular platinum cavities of 0.17 cm length and 0.05 diameter, the total volume (V) results to be 0.0063 cm^3.

The $n_{electrolysis}$ is obtained by the Faraday´s law:

$$n_{electrolysis} = \left(\frac{1}{z}\right)\frac{Q}{F}$$

where *Q* corresponds to the charge consumed during the electrolysis, *z* corresponds to the number of electron transfer per molecule (*z* =1, in this case) and *F* is a Faraday´s constant (96485.3 A s mol^{-1}).

Here it follows the table with the used values and the recorded spectra overtime and their ΔA_t plotting. The reported plotting are not perfectly linear in the earliest seconds due to a small delay betweem the optical and electrolysis measurements that were done separately and manually.

Table S3. Reported value used for the estimation of the Faradaic Efficiency. The molar absorptivity coefficient

Potential	Q (C)	$n_{electrolysis}$	ΔA	Δc (M)	n_{optics}	FE (%)
0.5V	1.71E-04	1.77E-09	0.14	3.66E-05	2.31E-10	13
0.6 V	2.33E-04	2.409E-09	0.31	7.94E-05	5.00E-10	21
0.7 V	3.27E-04	3.389E-09	0.43	1.10E-04	6.92E-10	20
0.9 V	5.10E-04	5.29E-09	0.42	1.09E-04	6.88E-10	13

(*ε)* value at 937 nm for the radical cation is equal to 2.29*10^4 $M^{-1}cm^{-1}$.

Figure S13. On the left: differential absorption spectra of circulene **C1** measured using honeycomb electrode after applying potential of 0.5 V (vs Fc/Fc^+) for 80 s; spectra were recorded at five-seconds intervals. On the right:

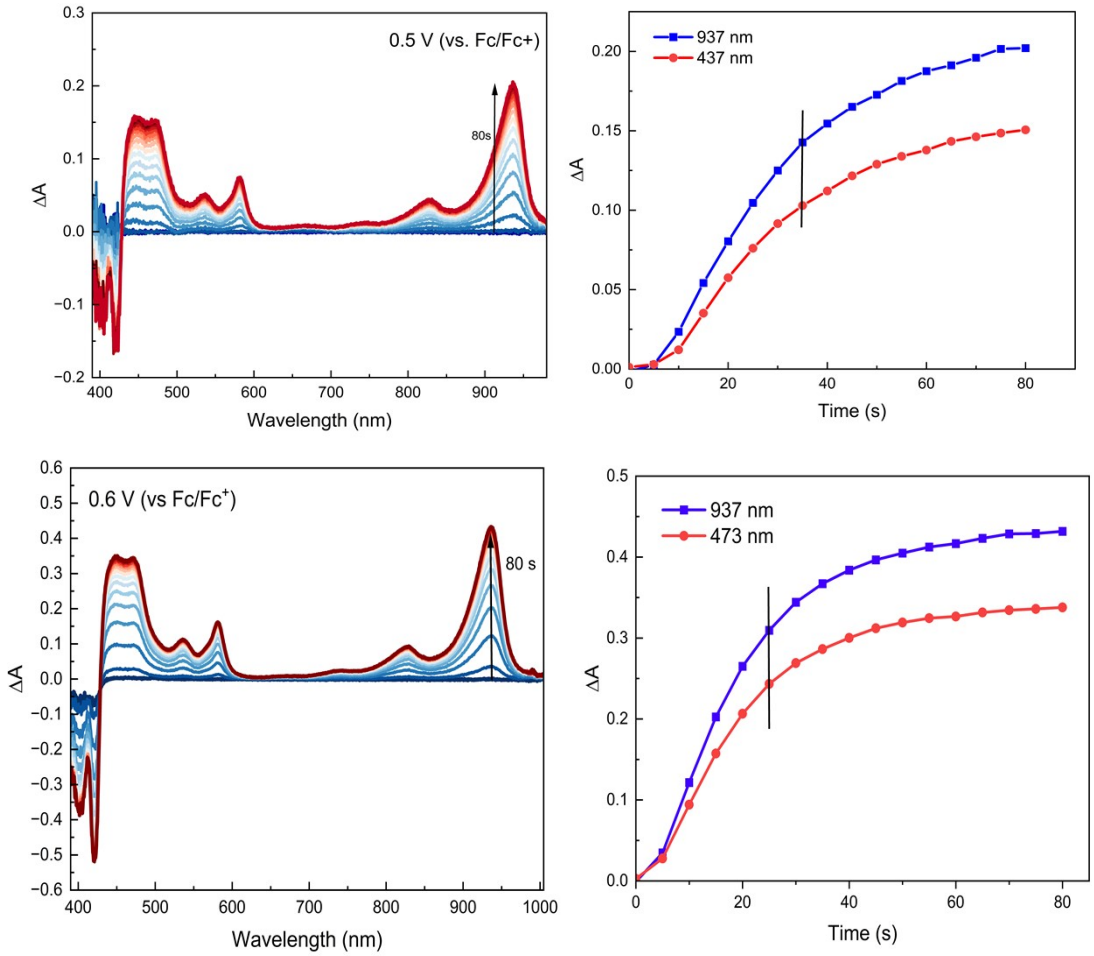

plotting of the differential absorption measured over time at 937 and 437 nm, applying 0.5 V. The black line indicates the point considered as saturation time.

Figure S14. On the left: differential absorption spectra of circulene **C1** measured using honeycomb electrode after applying potential of 0.6 V (vs Fc/Fc^+) for 80 s; spectra were recorded at five-seconds intervals. On the right: plotting of the differential absorption measured over time at 937 and 437 nm, applying 0.6 V. The black line indicates the point considered as saturation time.

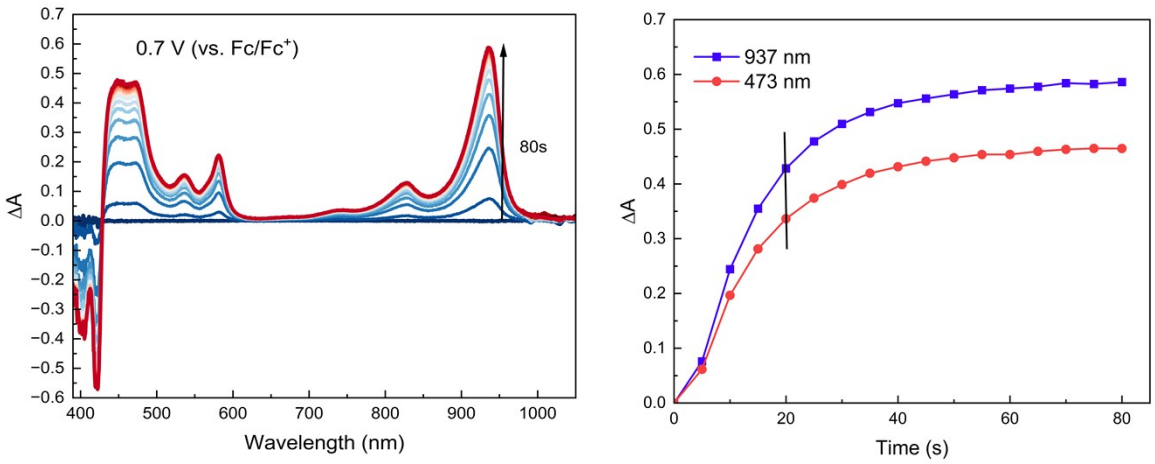

Figure S15. On the left: differential absorption spectra of circulene **C1** measured using honeycomb electrode after applying potential of 0.7 V (vs Fc/Fc^+) for 80 s; spectra were recorded at five-seconds intervals. On the right: plotting of the differential absorption measured over time at 937 and 437 nm, applying 0.7 V. The black line indicates the point considered as saturation time.

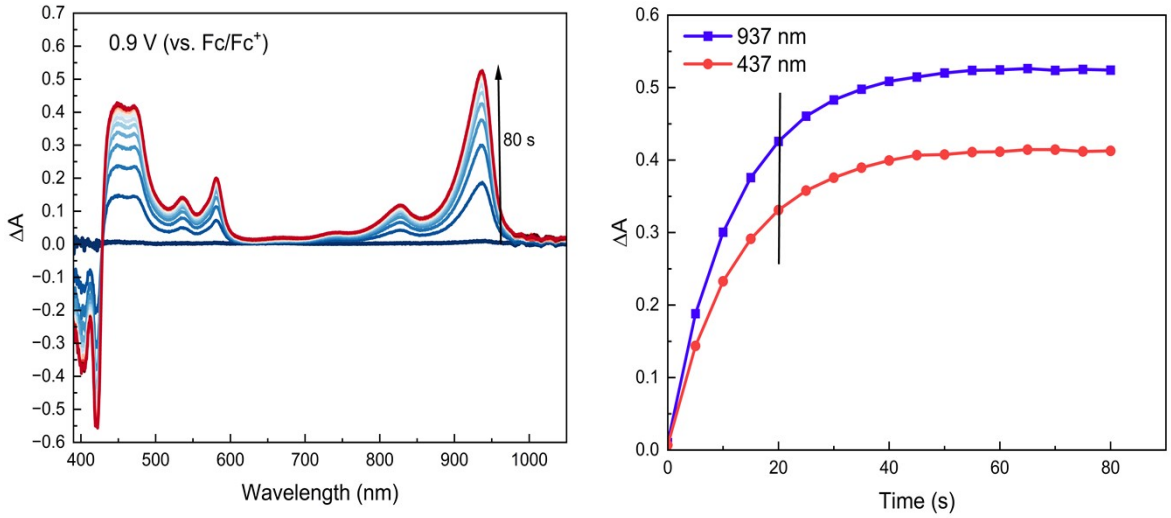

S16. On the left: differential absorption spectra of circulene **C1** measured using honeycomb electrode after applying potential of 0.9 V (vs Fc/Fc^+) for 80 s; spectra were recorded at five-seconds intervals. On the right:

plotting of the differential absorption measured over time at 937 and 437 nm, applying 0.9 V. The black line indicates the point considered as saturation time.

Theoretical calculations

Absorption and emission properties of neutral, cation, and dication circulenes were investigated with density functional theory atomistic simulations. We used GD3BJ-B3LYP[31–33] functional and 6-31+G(d).[34–36] All systems underwent geometrical optimization in dichloromethane implicit solvent followed by a frequency check. Absorption and emission were calculated with time-dependent density functional theory.[57] Particularly, for cation radical **C1** the emissive D_4 state was optimized by TD-DFT/GD3BJ-B3LYP/6-31+G(d) and vertical excitation $D_0 \rightarrow D_4$ was then calculated as the fluorescence wavelength. Simulations were carried out in the Gaussian 16 software package. ICSSzz plots were simulated according to Ref [58]. Also, we used RI-CC2[59-62] and ADC(2)[63,64] methods. For aromaticity studies, we used GIMIC software.[65-69]

All vibrational modes of final states were considered in the ISC and IC rate constant calculations. The method of calculations was described in details in Refs [70] and [71]. The method uses the general equation between the intramolecular vibrational relaxation width and the radiationless rate constant through the Lorentzian broadening. This method was applied many times to different kinds of molecules and gives the rate constants with high accuracy (within one order of magnitude). According to this model, the energy of the electronic excited state is converted in many combinations of vibrational mode excitation of final electronic states, irreversibly satisfying the energy conservation law as

$$k_{nr} = \frac{4}{\Gamma_{fn} \sum_{n} |V_{i0,fn}|^2},$$

where Γ_{fn} is a rate constant of intramolecular vibrational relaxation (which almost does not depend on type of molecule and nature of excited state and equals to ~10^{14} s^{-1}). The summation of different combinations of vibrational mode excitation was realized by using the dynamic programming algorithm described in the Ref [71]. The Strickler-Berg equation[41] was used for the k_r calculation by using the oscillator strength and the energy of electronic transition (extracted from RI-CC2 simulations) as

$$k_r(i \rightarrow f) = \frac{1}{1.5} f E_{if}^2.$$

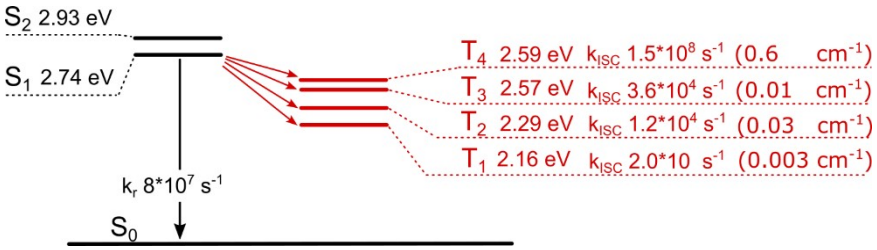

Figure S17. A Jablonski diagram for neutral circulene.

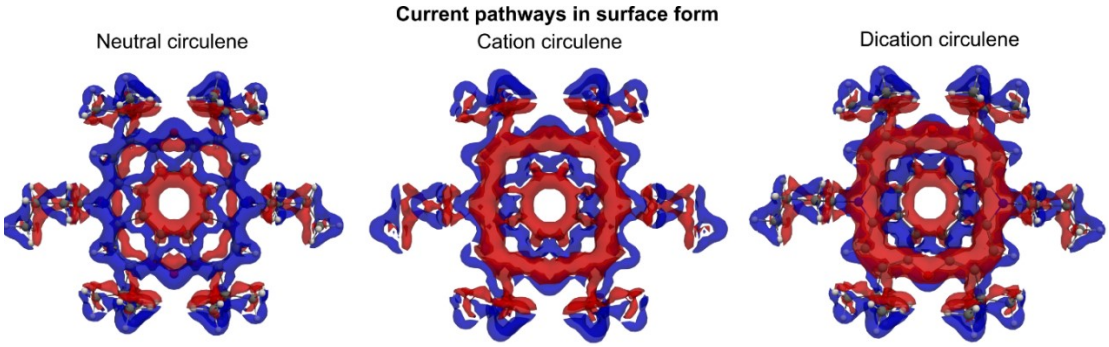

Figure S18. Current pathways for neutral molecule and its cation and dication counterparts.

Table S4. Absorption properties in neutral, cation and dication circulenes using TD-DFT/B3LYP+D3/6-31+G(d). Asterisk "*" marks wavelength and oscillator strength values simulated with RI-CC2/def2-SVP method.

Species	Transition	λ, nm	f	Assignment	<S²>
Neutral, q=0, S=1	S_0-S_1	416.88	0.0000	187 -> 189 0.70525	0.000
Cation, q=+1, S=2	D_0-D_1	4856.42 3543*	0.0061 0.03*	184B -> 188B -0.10357 186B -> 188B 0.99327	0.772
Cation, q=+1, S=2	D_0-D_2	4326.53 3351*	0.0335 0.0094*	187B -> 188B 0.99902	0.759
Cation, q=+1, S=2	D_0-D_3	3276.77 2138*	0.0000 0.0008*	185B -> 188B 0.99949	0.773
Cation, q=+1, S=2	D_0-D_4	936.47 795*	0.1048 0.1*	187A -> 189A 0.11429 184B -> 188B 0.98384	0.783
Dication, q=+2, S=1	S_0-S_1	4351.15	0.0096	186 -> 188 0.38355 187 -> 188 0.65153 187 <- 188 -0.26738	0.000
Dication, q=+2, S=1	S_0-S_2	2395.68	0.0000	185 -> 188 0.71004	0.000
Dication, q=+2, S=1	S_0-S_3	2308.23	0.0434	184 -> 188 0.17199 186 -> 188 0.60042 187 -> 188 -0.41763 186 <- 188 -0.16603 187 <- 188 0.19984	0.000
Dication, q=+2, S=1	S_0-S_4	713.21	0.2403	184 -> 188 0.67873 186 -> 188 -0.17654	0.000

Table S5. Emission properties in neutral, cation and dication circulenes using TD-DFT/B3LYP+D3/6-31+G(d)

Species	Transition	λ, nm	f	Assignment	<S²>
Neutral, q=0, S=1	S_1-S_0	528.95	0.0000	188 -> 189 0.70612	0.000
Neutral, q=0, S=1	S_2-S_0	452.63	0.5557	187 -> 189 0.70123	0.000
Cation, q=+1, S=2	D_4-D_0	1017.50	0.1501	184B -> 188B 0.98806	0.779
Dication, q=+2, S=1	S_4-S_0	798.22	0.3328	184 -> 188 0.68832 186 -> 188 0.16532	0.000

References

45 S. Stoll, A. Schweiger, EasySpin, a comprehensive software package for spectral simulation and analysis in EPR, *J. Magn. Reson.,* **2006**, *178*, 42–55.

46 F. Neese, F. Wennmohs, U. Becker, C. Riplinger, The ORCA quantum chemistry program package, *J. Chem. Phys.,* **2020**, *152*, 224108.

47 F. Neese, The ORCA program system, *WIREs Comput. Mol. Sci.,* **2012**, *2*, 73–78.

48 F. Neese, Software update: The ORCA program system—Version 5.0, *WIREs Comput. Mol. Sci.,* **2022**, *12*, e1606.

49 Rigaku Corporation, **2025**.

50 G. M. Sheldrick, SHELXT – Integrated space-group and crystal-structure determination, *Acta Crystallogr. Sect. A Found. Adv.,* **2015**, *71*, 3–8.

51 O. V. Dolomanov, L. J. Bourhis, R. J. Gildea, J. A. K. Howard, H. Puschmann, OLEX2 : a complete structure solution, refinement and analysis program, *J. Appl. Crystallogr.,* **2009**, *42*, 339–341.

52 G. M. Sheldrick, Crystal structure refinement with SHELXL, *Acta Crystallogr. Sect. C Struct. Chem.,* **2015**, *71*, 3–8.

53 L.-M. Peng, Electron atomic scattering factors and scattering potentials of crystals, *Micron,* **1999**, *30*, 625–648.

54 F. H. Allen, I. J. Bruno, Bond lengths in organic and metal-organic compounds revisited: X —H bond lengths from neutron diffraction data, *Acta Crystallogr. Sect. B Struct. Sci.,* **2010**, *66*, 380–386.

55 L. J. Farrugia, WinGX and ORTEP for Windows : an update, *J. Appl. Crystallogr.,* **2012**, *45*, 849–854.

56 C. F. Macrae, I. Sovago, S. J. Cottrell, P. T. A. Galek, P. McCabe, E. Pidcock, M. Platings, G. P. Shields, J. S. Stevens, M. Towler, P. A. Wood, Mercury 4.0 : from visualization to analysis, design and prediction, *J. Appl. Crystallogr.,* **2020**, *53*, 226–235.

57 R. Bauernschmitt, R. Ahlrichs, Treatment of electronic excitations within the adiabatic approximation of time dependent density functional theory, *Chem. Phys. Lett.,* **1996**, *256*, 454–464.

58 Z. Liu, T. Lu, Q. Chen, An sp-hybridized all-carboatomic ring, cyclo[18]carbon: Bonding character, electron delocalization, and aromaticity, *Carbon N. Y.,* **2020**, *165*, 468–475.

59 O. Christiansen, H. Koch, P. Jørgensen, The second-order approximate coupled cluster singles and doubles model CC2, *Chem. Phys. Lett.,* **1995**, *243*, 409–418.

60 F. Weigend, M. Häser, H. Patzelt, R. Ahlrichs, RI-MP2: optimized auxiliary basis sets and demonstration of efficiency, *Chem. Phys. Lett.,* **1998**, *294*, 143–152.

61 C. Hättig, F. Weigend, CC2 excitation energy calculations on large molecules using the resolution of the identity approximation, *J. Chem. Phys.,* **2000**, *113*, 5154–5161.

62 C. Hättig, Structure Optimizations for Excited States with Correlated Second-Order Methods: CC2 and ADC(2), *Adv. Quantum Chem.,* **2005**, *50*, 37–60.

63 J. Schirmer, Beyond the random-phase approximation: A new approximation scheme for the polarization propagator, *Phys. Rev. A,* **1982**, *26*, 2395.

64 A. Trofimov, J. Schirmer, An efficient polarization propagator approach to valence electron excitation spectra, *J. Phys. B At. Mol. Opt. Phys.,* **1995**, *28*, 2299.

65 H. Fliegl, R. Valiev, F. Pichierri, D. Sundholm, Theoretical studies as a tool for understanding the aromatic character of porphyrinoid compounds, *SPR - Chem. Model.*, **2018**, pp. 1–42.

66 D. Sundholm, H. Fliegl, R.J.F. Berger, Calculations of magnetically induced current densities: theory and applications, *WIREs Comput. Mol. Sci.,* **2016**, *6*, 639–678.

67 H. Fliegl, D. Sundholm, Aromatic pathways of porphins, chlorins, and bacteriochlorins , *The Journal of organic chemistry,* **2012**, *77(7)*, 3408-3414.

68 J. Jusélius, D. Sundholm, J. Gauss, Calculation of current densities using gauge-including atomic orbitals, *The*

Journal of chemical physics, **2004**, *121(9)*, 3952-3963.

69 H. Fliegl, S. Taubert, O. Lehtonen, D. Sundholm, The gauge including magnetically induced current method, *Phys. Chem. Chem. Phys.,* **2011**, *13*, 20500.

70 R. R. Valiev, B. S. Merzlikin, R. T. Nasibullin, A. Kurtzevitch, V. N. Cherepanov, R. R. Ramazanov, D. Sundholm, T. Kurtén, Internal conversion rate constant calculations considering Duschinsky, anharmonic and Herzberg–Teller effects, *Phys. Chem. Chem. Phys.,* **2023**, 25, 6406–6415.

71 R. R. Valiev, B. S. Merzlikin, R. T. Nasibullin, D. Sundholm, T. Kurtén, The role of X–H bonds (X = C, N and O) in internal conversion processes: dibenzoterrylene as an example, *Phys. Chem. Chem. Phys.,* **2025**, *27*, 16853–16864.